The Effects of an Engineered Cation Site on the Structure, Activity, and EPR Properties of Cytochrome *c* Peroxidase[†]

Christopher A. Bonagura, M. Sundaramoorthy, B. Bhaskar, and Thomas L. Poulos*

Departments of Molecular Biology & Biochemistry and of Physiology & Biophysics, University of California, Irvine, California 92697-3900

Received December 21, 1998; Revised Manuscript Received February 4, 1999

ABSTRACT: Earlier work [Bonagura et al. (1996) *Biochemistry 35*, 6107] showed that the K^+ site found in the proximal pocket of ascorbate peroxidase (APX) could be engineered into cytochrome *c* peroxidase (CCP). Binding of K^+ at the engineered site results in a loss in activity and destabilization of the CCP compound I Trp191 cationic radical owing to long-range electrostatic effects. The engineered CCP mutant crystal structure has been refined to 1.5 Å using data obtained at cryogenic temperatures which provides a more detailed basis for comparison with the naturally occurring K^+ site in APX. The characteristic EPR signal associated with the Trp191 radical becomes progressively weaker as K^+ is added, which correlates well with the loss in enzyme activity as $[K^+]$ is increased. These results coupled with stopped-flow studies support our earlier conclusions that the loss in activity and EPR signal is due to destabilization of the Trp191 cationic radical.

Heme peroxidases catalyze the oxidation of a variety of substrates at the expense of hydrogen peroxide in the following multistep reaction cycle:

$$Fe^{3+}\ R + H_2O_2 \rightarrow \underset{\text{compound I}}{Fe^{4+}{=}O\quad R^{\bullet}} + H_2O$$

$$Fe^{4+}{=}O\ R^{\bullet} + S \rightarrow \underset{\text{compound II}}{Fe^{4+}{=}O\ R} + S^{\bullet}$$

$$Fe^{4+}{=}O\ R + S \rightarrow Fe^{3+}\ R + S^{\bullet} + H_2O$$

The enzyme is first oxidized by peroxide to give compound I. One electron is removed from the heme iron to give the oxyferryl center ($Fe^{4+}{=}O$), and a second electron is removed from an active site group, R, in the above scheme. Compound I is then reduced back to the resting state by two substrate molecules, S, in two successive one-electron-transfer events. In most heme peroxidases, $R^{\bullet}$ is a porphyrin π cation radical (*1*). However, cytochrome *c* peroxidase (CCP)[1] does not form a porphyrin radical in compound I, but instead forms a stable radical centered on an amino acid side chain (*2*). This was later shown to be Trp191 (*3*, *4*), an amino acid residue that is part of the His175−Asp235−Trp191 proximal triad that helps to regulate the redox potential of the heme iron (*5*).

Most heme peroxidases oxidize small aromatic molecules. It is generally accepted that these substrates interact directly with the exposed δ-meso heme edge (*6*) leading to direct electron transfer to the porphyrin π cation radical followed by a second electron transfer to the $Fe^{4+}{=}O$ center. While cytochrome *c* peroxidase (CCP) is very similar in structure to other heme peroxidases, its specificity toward reduced cytochrome *c* (ferrocyt *c*) as the reducing substrate has resulted in the evolution of a significantly different electron-transfer mechanism. CCP interacts with ferrocyt *c* by forming a specific protein−protein complex (*2*, *7*). The crystal structure of the cytochrome *c*−CCP noncovalent complex (*8*) shows that the most direct route of electron transfer involves Trp191. Trp191 is situated perpendicular to and just beneath the CCP heme, directly adjacent and parallel to the proximal His heme ligand. The cyt *c*−CCP structure shows that the cytochrome *c* heme contacts CCP Ala194, which provides the shortest route of electron transfer to the Trp191 radical.

Once the crystal structures of several peroxidases became available, a simple explanation was provided for why CCP forms a Trp cation radical while other peroxidases form porphyrin π cation radicals. The extracellular peroxidases do not have a Trp at the same position as Trp191 in CCP, but instead have either a Phe or an aliphatic residue. It seemed reasonable to conclude that in CCP the Trp191 residue forms a more stable radical while the relatively higher redox potential of Phe precludes oxidation of the Phe and instead leads to oxidation of the heme porphyrin. However, the crystal structure (*9*) and subsequent characterization of Trp179 in ascorbate peroxidase (APX) proved this view to be incorrect. Trp179 in APX is in exactly the same position as is Trp191 in CCP, yet APX forms a porphyrin π cation radical similar to other heme peroxidases. In addition, the

[†] This research was supported in part by National Institutes of Health Grant GM42615 and National Science Foundation Grant MCB-9807798.

* To whom correspondence should be addressed at the Department of Molecular Biology & Biochemistry. E-mail: poulos@uci.edu. FAX: (949) 824-3280.

[1] Abbreviations: CCP, cytochrome *c* peroxidase; APX, ascorbate peroxidase; EPR, electron paramagnetic resonance spectroscopy; cyt *c*, cytochrome *c* from horse heart; ferrocyt *c*, reduced cytochrome *c*; DMI, 1,2-dimethylimidazolium.

10.1021/bi982996k CCC: $18.00
Published on Web 04/07/1999

Trp179Phe APX mutant shows that the proximal Trp is not essential for APX activity (*10*) while the same mutation in CCP leads to a near complete loss in activity (*11*).

It thus became clear that in CCP the protein environment surrounding Trp191 somehow modulates the reactivity of radical formation. One possibility is that the protein provides an electronegative environment designed to stabilize the positive charge that develops on the Trp191 cation radical in compound I. Indeed, it now has been shown that the Trp191Gly mutant prefers to bind cations at this site (*12, 13*). The reason that APX does not form a Trp179 radical was postulated to be due to two factors. First, as in CCP, the local environment also attenuates the electrostatic potential around Trp179. In the case of APX, the local environment is more electropositive than in CCP, which is supported by electrostatic potential calculations that we reported previously (*14*) and confirmed by a more sophisticated analysis (*15*). Second, APX, as well as all extracellular peroxidases, has a cation bound about 8 Å from the proximal Trp. This was postulated to destabilize a cationic Trp radical in APX via long-range electrostatic effects (*16*). In APX, the proximal cation binding site is occupied by potassium, while in other peroxidases, the cation is calcium.

To test the role of the cation binding site in the regulation of CCP Trp191 reactivity, the APX cation site was engineered into CCP (*14*). Characterization of the engineered CCP proximal cation binding mutant, CCPK2, by X-ray crystallography, kinetic analysis, and EPR spectroscopy showed that potassium does bind to the CCP mutant at the intended engineered site. This mutant was shown to exhibit a dramatic decrease in the level of activity, and the characteristic EPR signal of the Trp191 radical is greatly diminished in potassium phosphate buffer. From these observations and electrostatic calculations, we concluded that the bound cation does destabilize the Trp191 radical as predicted.

Further analysis of the CCP cation mutant presented here has led to the finding that the mutations themselves as well as the bound cation affect both enzyme activity and the EPR properties of compound I. This has led to a more extensive analysis of the CCPK2 cation mutant ± various cations, which includes the potassium-dependent behavior of this mutant in single-turnover and steady-state kinetic analyses, and EPR spectroscopy. A higher resolution 1.5 Å cryogenic structure of the CCPK2 also enables a more detailed and accurate comparison between the engineered CCP proximal cation binding site with the APX site from which it was designed.

MATERIALS AND METHODS

Protein Expression and Purification. The cation mutant used in the present study is designated CCPK2. This mutant has five amino acid substitutions corresponding to the proximal cation binding loop in APX. CCPK2 is altered at the following residue positions: A176T, G192T, A194N, T199D, and G201S as previously reported (*14*). Both wild-type CCP (WTCCP) and CCPK2 proteins were expressed using a T7 promoter in *E. coli* BL21 cells induced initially at $OD_{600} = 0.8$ cell density with 750 μM IPTG for 4 h. Protein was purified as previously described by Fishel et al. (*17*) and Choudhury et al. (*18*), with the exception of an FPLC anion exchange step introduced using similar gradient parameters. After gel filtration on a 2 L G-75 column, and a heme incorporation step by standard pH shift, CCPK2 was loaded onto a 5 mL HiTrap Q anion exchange column in 50 mM potassium phosphate (KPO_4), pH 6.0, using a Pharmacia Biotech FPLC. The protein was eluted by stepping the gradient first to 80 mM then to 130 mM buffer followed by a linear gradient from 130 mM to 500 mM buffer at pH 6.0. For CCPK2, the FPLC step was also used prior to heme incorporation to separate any apoprotein from the large amount of low-spin holoprotein (~40%) produced during expression. After heme incorporation and anion exchange chromatography, CCP was twice crystallized by dialysis against Milli-Q water before being stored at −80 °C in H_2O. CCP concentration was estimated spectrophotometrically using an extinction coefficient $E_{408\ nm} = 94\ mM^{-1}\ cm^{-1}$.

Steady-State Activity Assays. For substrate titration assays, the steady-state oxidation of dithionite-reduced horse heart cytochrome *c* (ferrocyt *c*) was measured at 22 °C in a Cary 3E spectrophotometer using $\Delta E_{550\ nm} = 19.6\ mM^{-1}\ cm^{-1}$. The final reaction conditions (*19*) consisted of 180 μM H_2O_2, and 75 pM WTCCP or 75 nM CCPK2, in 50 mM Tris−PO_4, pH 6.0. The initial linear region of the reaction slope was recorded and taken as a least-squares fit using Cary Varian 01.00(6) software running on Windows 95. All data points reported in this paper reflect the average of at least three independent slopes averaged, and were plotted in Sigmaplot 4.0.

The following assay conditions were employed to measure steady-state activity as a function of cation concentration. CCPK2 was added to 5 mM Tris−PO_4, pH 6.0, initially containing potassium ion, or other cations, at various concentrations, and then 180 μM hydrogen peroxide and 40 μM ferrocyt *c* were added to begin the reaction. Tris−PO_4 is 1 M Tris base (Boehringer Mannheim) equilibrated to pH 6.0 with ion-free phosphoric acid purchased from Aldrich Chemicals. Horse heart cytochrome *c* (catalog no. 7752) and hydrogen peroxide as a 30% w/v stabilized solution were purchased from Sigma Chemicals. Hydrogen peroxide stocks were standardized with $KMnO_4$ using the method of Fowler and Bright (*20*).

Spectral Titrations with 1,2-Dimethylimidazolium (DMI). Binding assays were performed by difference absorption spectroscopy using a Cary 3E UV−visible spectrophotometer set at 20 °C. Stock solutions of 1 M 1,2-dimethylimidazolium (DMI) were prepared with 100 mM Bis-tris-propane/MES, pH 6.0. Stock frozen protein solutions of WTCCP and CCPK2 were prepared in 100 mM Bis-tris-propane/MES, pH 6.0. An aliquot of the DMI stock solution (10 μL of 1 M for CCPK2 and 10 μL of 5 M for WTCCP) was added to the cuvette and allowed to equilibrate with stirring before the change in the absorption spectrum was recorded. Dissociation constants (K_d) were determined from Scatchard plots based on measuring the difference absorbance at the Soret maximum of the heme.

Stopped-Flow Kinetics. Stopped-flow kinetics were measured at a single wavelength using a Hi-Tech Model SF-51 stopped-flow SHU linked to a Hi-Tech SU-40 spectrophotometer. The output was monitored and recorded on a Compaq PC for kinetic analysis using Hi-Tech IS-1 software suite version 1.0.

To evaluate the single electron-transfer rate from horse heart ferrocyt *c* to the CCP compound I, the following reaction conditions were employed. CCPK2 or WTCCP compound I at an initial concentration of 4.0 μM was formed by addition of an equal volume of 4.6 μM H_2O_2. Then 2 μM CCP compound I in one syringe was mixed with 1.0 μM reduced ferrocyt *c* in the other syringe. The buffer used was 0.1 M Tris−PO_4, pH 6.0, with or without 5 mM KCl present. The high ionic strength buffer used slows the WTCCP reaction sufficiently to enable the reaction to be followed on the time-scale of the stopped flow (*21*). Using this protocol, CCP compound I is in 2-fold excess over ferrocyt *c* so all of substrate electrons are delivered to compound I, which gives monophasic kinetics (*22*). Oxidation of ferrocyt *c* was monitored at 416 nm, an isosbestic point for resting CCP ferric and oxyferryl compound I.

Electron Paramagnetic Resonance Spectroscopy. EPR spectra were recorded on a Bruker ESP300 spectrometer equipped with an Air Products LTR3 liquid helium cryostat at 8.0 K. Experimental conditions used to record the CCPK2 Trp191 cation radical compound I spectra were as follows: microwave frequency, 9.48 GHz; microwave power, 0.5 mW; modulation amplitude, 4.57 G; modulation frequency, 1000 kHz; field sweep rate, 11.92 G/s; time constant, 0.0256 ms; receiver gain, 5.0×10^4. The resulting scans were plotted by Sigma Plot version 4.0. WTCCP and CCPK2 compound I were formed at 0 °C on ice in quartz EPR tubes (Wilmad Glass), and after 80 s the samples were frozen in liquid nitrogen.

Crystallization, X-ray Data Collection, and Structure Refinement. Diffraction-quality crystals were prepared in 30% 2-methyl-2,4-pentanediol, 50 mM KPO_4, pH 6.0, according to (*23*) as later modified by (*24*). A lower initial concentration of CCPK2 was used, 200 μM (~6.4 mg/mL), than previously reported in order to grow smaller 0.2 mm crystals from touch seeding. This smaller size crystal was necessary for proper cryogenic freezing and to avoid twinning during crystal growth. X-ray intensity data were collected from a single crystal of CCPK2, flash-frozen directly in the N_2 stream. Data were collected at Stanford Synchrotron Radiation Laboratory (SSRL) beamline 7.01, using a Mar Research imaging plate (Mar 30). Initial image processing, indexing, and integration were performed with Denzo version 1.9.1, and the integrated data were scaled using ScalePack version 1.9.0 (*25*).

The room-temperature CCPK2 structure reported previously (*14*) was used as the starting model for this refinement. The unit cell lost 6.4% in volume upon freezing as compared to room-temperature crystals. The model was placed into the smaller cryogenic unit cell using 10 cycles of rigid-body refinement (50.0−2.5 Å) as implemented in XPLOR version 3.851 (*26*). The *R*-factor at this point was 26%. Next, 5% of the data were set aside to follow R_{free} for cross-validation analysis (*27*). To begin refinement of the model, simulated annealing starting at 3000K as implemented in XPLOR was used to remove any previous model bias.

$F_o - F_c$ difference maps and $2F_o - F_c$ electron density maps were then calculated using this model as input. The model was rebuilt to better fit changes in the difference maps using Tom version 3.1 (*28*). The conventional refinement process involved model building and then positional refinement for 30 cycles followed by *B*-factor refinement for 10 cycles. Alternative conformations were modeled for residue positions Arg48, Lys123, Arg127, and Arg166, and water molecules 427 and 768. In addition, 380 new ordered solvent molecules were added to the molecular model. X-ray intensity data processing and refinement statistics are summarized in Table 1.

Table 1: Summary of Data Collection Statistics and Crystallographic Refinement

Summary of Data Collection	
no. of unique reflections	64691
no. of observations ($>1\sigma$)	240248
total no. of observations	245706
completeness, full data set (%)	96.0
completeness in last shell (%)	88.4
I/σ from 1.52 to 1.50 Å	2.07
R_{sym}[a]	0.056
unit cell dimensions	$a = 106.72$ Å
	$b = 75.53$ Å
	$c = 51.26$ Å
Statistics for Refinement	
resolution range	10−1.5 Å
no. of reflections used ($I/\sigma > 2.0$)	55347
R_{free}	23.4
R[b] (%)	19.7
rms deviation of bond lengths (Å)	0.007
rms deviation of bond angles (deg)	1.304
no. of waters added	380

[a] $R_{sym} = \Sigma|I - \langle I\rangle|/\Sigma I$. [b] $R = \Sigma F_o - F_c/\Sigma F_o$. [c] R_{free} calculated from 5% data set aside.

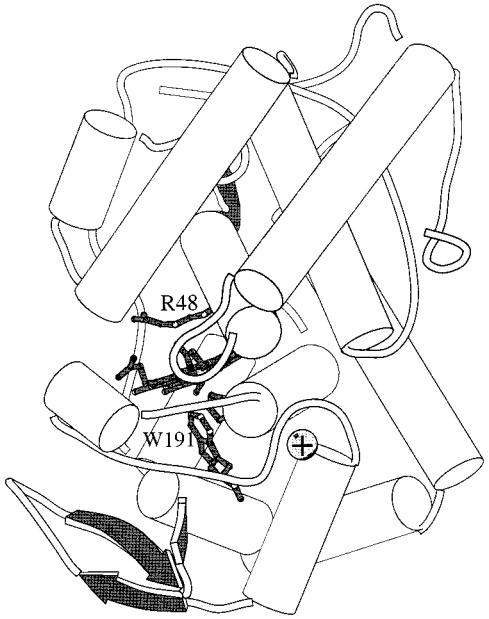

FIGURE 1: Model of CCPK2 depicting the relationship of the engineered proximal cation binding site, Trp191, and the CCP heme. The distal active site arginine is also included.

RESULTS

Crystal Structure of CCPK2 at 1.5 Å Resolution. The higher resolution and improved data quality obtained at SSRL have provided a more accurate description of the engineered cation site. During the course of refinement, no constraints or restraints were used between the ligand and cation in order to provide an unbiased set of ligand−cation parameters. The location of the engineered cation site is shown in Figure 1, while Figure 2 presents a close-up view of the engineered

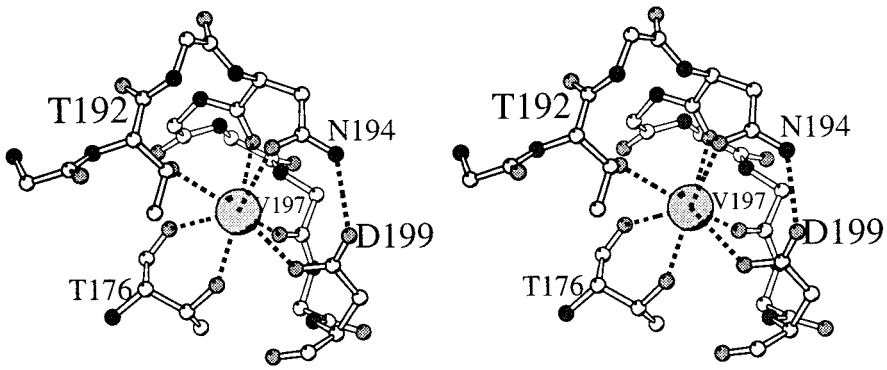

FIGURE 2: Stereoview of the proximal cation binding site of CCPK2 at 1.5 Å resolution. The high-resolution structure depicts a more accurate model of the potassium binding site. The measured distances from this site are reported in Table 2.

Table 2: Comparison of Cation to Ligand Distances[a]

residue in CCP (APX)	distance in Å	
	CCPK2	APX
Thr176 (169) OG1	2.65	2.57
Thr176 (169) C═O	2.62	2.88
Thr192 (180) OG1	2.90	2.96
Asn194 (182) C═O	2.76	2.77
Asn194 (182) OD1	2.87	2.74
Val197 (185) C═O	2.72	2.61
Asp199 (187) OD1	3.02	2.99
H-bond from Asn194 ND2 (182) to Asp199 OD2 (187)	2.92	2.86

[a] Numbers in parentheses = corresponding residue in APX.

site. In addition to the better CCPK2 structure, the APX structure has been more highly refined using a 1.8 Å cryogenic data set (*29*). This enables a more accurate and direct comparison of bond distances and bond angles between the CCPK2 and APX proximal cation binding loops, as shown in Table 2. An omit $F_o - F_c$ difference map shows a 34 σ positive difference peak, clearly indicating a bound cation. When modeled as K^+ with full occupancy, the temperature factor refines to 9.45 Å^2, which compares favorably with the 9.68−11.75 Å^2 range for the seven oxygen ligand atoms to the cation.

One of the more important new observations that these data have provided is a hydrogen bond between the side chain amino group on Asn194 and the peptide carbonyl oxygen of Asp199 (Figure 2). This critical hydrogen bond was not apparent in the lower resolution CCPK2 structure we previously reported. This same hydrogen bond also is present in APX. It is significant because this bond no doubt imparts some stability to the cation loop, because two mutants we have constructed that lack this hydrogen bond have a marked decrease in stability (unpublished results). Even more importantly, this hydrogen bond helps to orient the carbonyl oxygen of the Asn194 side chain to point toward and become a ligand to the cation.

The current model also shows a number of interesting alternative side-chain conformations that reveal greater detail about function. In particular, Arg48, a residue in the distal pocket involved in the formation and stabilization of compound I, is obviously in two positions we have termed "*in*" and "*out*". The *out* conformation is the same as the room temperature 1.7 Å structure of CCP (*30*) while the *in* conformation is similar to what is found in compound I (*31, 32*) and the fluoride complex (*33*). The *in* conformation

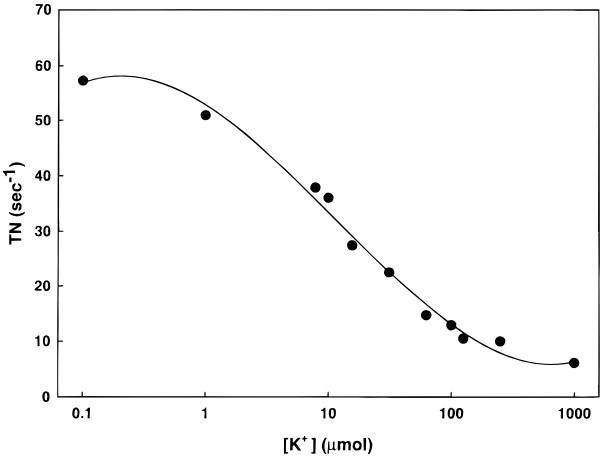

FIGURE 3: Steady-state activity assay of CCPK2 at various concentrations of K^+. Assays were carried out in 5 mM Tris−PO_4, pH 6.0, 180 μM hydrogen peroxide, and 40 μM ferrocyt *c* at the indicated K^+ concentration. From this curve the K_d is estimated to be 20 μM.

enables Arg48 to directly interact with ligands coordinated to the heme iron or, in the case of the high-spin ferric complex, to an ordered water molecule situated over the iron.

Steady-State Kinetics. In the presence of high concentrations of K^+, the activity for CCPK2 is ~1% of WTCCP, while in the absence of any added cations the activity is ~10% of WTCCP. This indicates that the mutations themselves lead to a 10-fold loss in activity while the addition of K^+ leads to another 10-fold loss in activity. This provides a simple method for estimating the K_d for potassium binding by measuring activity vs [K^+]. As shown in Figure 3, a typical sigmoid titration curve of turnover versus [K^+] is obtained, giving an estimated K_d of 20 μM.

The Eadie−Hofstee plots for both WTCCP and CCPK2 in the absence of K^+ (Figure 4a,b) give very similar and expected biphasic kinetics which have been attributed to two binding sites for ferrocyt *c* (*34*). The two K_m values for WTCCP are 3.6 and 29.7 μM to be compared with 1.1 and 20.6 μM for CCPK2. Moreover, the transition point between the two slopes occurs near 9 μM ferrocyt *c* for both WTCCP and CCPK2. To the extent that K_m values can be correlated with true dissociation constants, these similarities indicate that the interaction between ferrocyt *c* and CCP is similar in both WTCCP and CCPK2. Nevertheless, because the kinetics of CCP are complex, it is useful to have a nonkinetic estimate on the interaction between CCP and cyt *c*. We therefore utilized an affinity chromatography method (*35*) to estimate

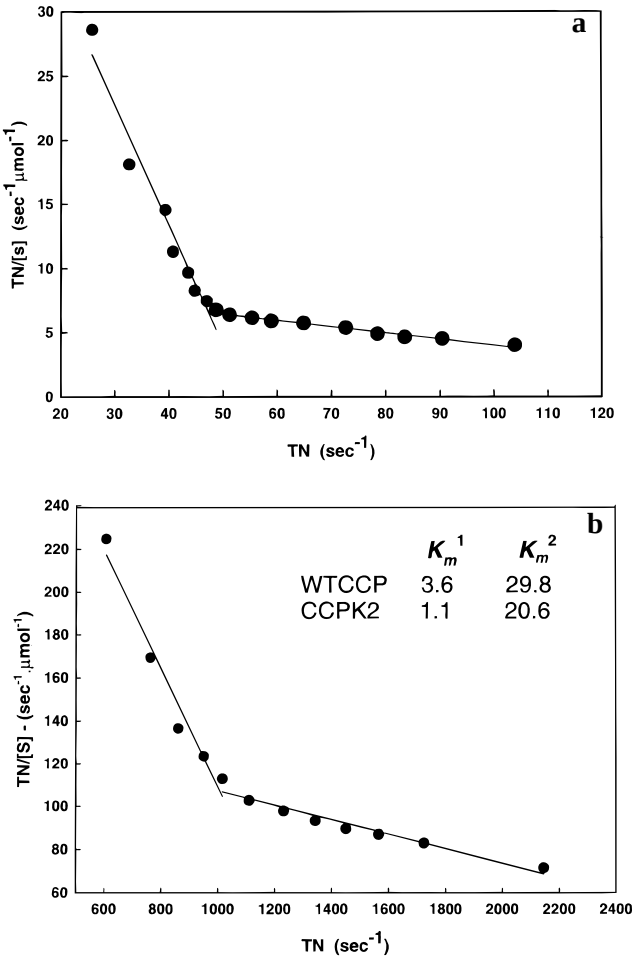

FIGURE 4: Eadie−Hofstee plots of WTCCP and CCPK2 steady-state turnover of horse heart ferrocyt *c*. Assays were carried out in 5 mM Tris−PO_4, pH 6.0, 180 μM hydrogen peroxide, and varying concentrations of ferrocyt *c*. The straight lines were obtained from linear regression fits to the data.

the relative affinity of WTCCP and CCPK2 for cyt *c* immobilized on a chromatographic support. In this method, CCP is chromatographed over a column to which yeast cyt *c* is covalently attached to the chromatographic resin via an S−S bond. CCP binds to the immobilized cyt *c* at low ionic strength and then is eluted at increasing salt concentrations. CCPK2 began to elute at 50 mM phosphate buffer, pH 6.0, while WTCCP did not elute from the column until ~100 mM. Therefore, CCPK2 has a weaker affinity for cyt *c* than does WTCCP.

Stopped-Flow Kinetics. To determine which steps in the catalytic cycle are impaired in CCPK2, rate constants for the elementary steps were determined using stopped-flow spectroscopy. We have already determined the rate of compound I formation to be 1.8×10^7 s^{-1} for CCPK2, which is very close to the value of 3.0×10^7 s^{-1} for WTCCP compound I formation (*14*). This demonstrates that the catalytic machinery required for compound I formation functions normally in CCPK2. We next determined the rate of ferrocyt *c* oxidation by compound I. In these single-turnover experiments, CCP compound I is in 2-fold excess over ferrocyt *c*. Under these conditions, each molecule of CCP will react with one molecule of ferrocyt *c*, leading to the one-electron reduction of compound I (*22*). As shown in Table 3, the oxidation of ferrocyt *c* in CCPK2 in the

Table 3: Rate of Oxidation of Ferrocyt *c* by CCP Compound I[a]

compound I	k_{obs} (s^{-1}) measured at 416 nm
WTCCP	80.88
WTCCP + KCl	78.06
CCPK2	7.49
CCPK2 + KCl	0.92

[a] A 2-fold excess of either CCPK2 or WTCCP compound I was mixed with an equal volume of ferrocyt *c* in a stopped flow and the rate of ferrocyt *c* oxidation measured at 416 nm.

absence of K^+ is 9.3% of the rate obtained for WTCCP and drops to 1.1% when K^+ is added. There is no effect of K^+ addition on the WTCCP activity under these conditions. These results correlate well with the steady-state kinetic observations and demonstrate that electron transfer from ferrocyt *c* is lowered in CCPK2 both with and without the addition of potassium. However, the lower electron-transfer rate upon addition of K^+ clearly demonstrates the potassium-dependent behavior of CCPK2.

EPR Spectroscopy. If the addition of K^+ is diminishing the stability of the Trp191 cation radical as postulated by long-range electrostatic effects, then the EPR signal of compound I should be titratable with the addition of cations. The EPR spectra of CCPK2 compound I at $g = 2.01-2.04$ are shown Figure 5a as a function of increasing amounts of potassium. It is clear that the EPR signal grows progressively weaker as [K^+] increases. The close parallel in the loss of activity and the diminishing EPR signal supports our earlier conclusions that activity loss is due to an electrostatic effect which destabilizes the Trp191 cation radical in the presence of bound potassium.

Figure 5b illustrates the effects that 10 mM LiCl, NaCl, CsCl, and $CaCl_2$ have on the CCPK2 Trp radical intensity, as compared to the intensity of CCPK2 recorded in the presence of K^+. There is moderate ion selectivity that correlates with ionic radius. For example, the smallest ion, Li^+, and the largest, Cs^+, have minimal effects on the EPR signal while the closest homologue to K^+, Na^+, is nearly but not quite as effective as K^+. Such moderate specificity is not unexpected since the CCP cation site was engineered to specifically mimic the APX K^+ site. Also shown are the high concentration end point effects of Na^+, Li^+, Cs^+, and Ca^{2+} ions in steady-state activity assay. The obvious trend with these several cations tested is that the activity, like the EPR signal, also is dependent on the cation ionic radius. The only inconsistency is the ability of Cs^+ to reduce activity to a greater extent than it reduces the EPR signal.

Cause of Activity Loss in the Absence of K^+. The results presented here and in our earlier work (*14*) support the view that the binding of K^+ causes an electrostatic destabilization of the Trp191 cation radical, resulting in a corresponding loss in activity. The reason the mutations alone lead to a large drop in activity and the compound I EPR Trp191 signal remains problematic. The affinity chromatography results indicate that CCPK2 does not bind as well to cyt *c* as WTCCP which could explain, in part, the loss in electron-transfer function. It nevertheless is clear that the mutations themselves have somehow altered the stability of the Trp191 radical.

Recent work by Cao et al. (*36*) provides a possible explanation. These authors have shown that CCP exists in an "open" and "closed" conformation and that the two forms

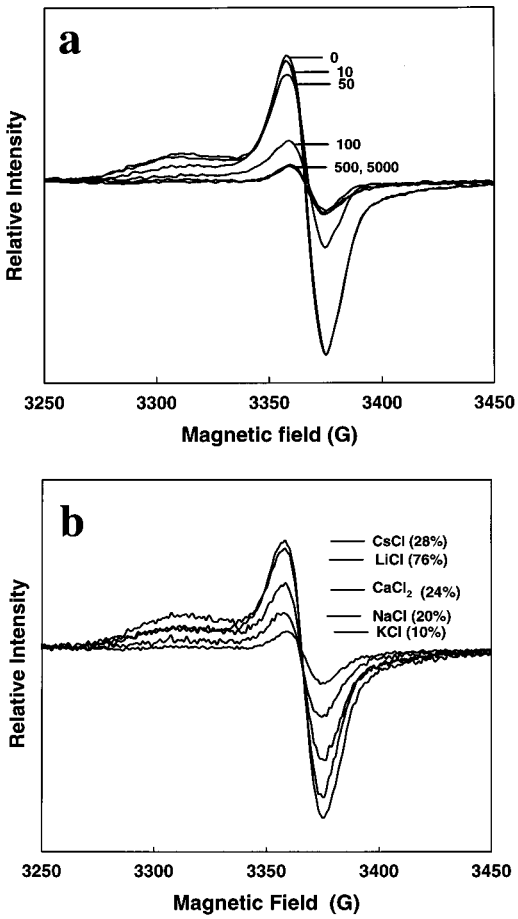

FIGURE 5: EPR spectra of the Trp191 cation radical signal of CCPK2 compound I as a function of K^+ concentration (a) and metal ion type (b). The EPR signal in the absence of any added cations is approximately 10-fold weaker than for WTCCP which correlates with the 10-fold lower activity. The numbers in parentheses in panel b are the percentage of steady-state activity remaining after addition of a 10 mM aliquot of the indicated cation. With the exception of CsCl, there is a correlation between loss in EPR signal and loss in activity.

are in equilibrium. The closed form has Trp191 in its native position observed in the crystal structures while in the open form, Trp191 moves ≈10 Å to the molecular surface owing to a large movement of the surface loop consisting of residues 190−195. Moreover, these authors have found that in the open conformation the now void Trp191 site can bind imidazole cations. This further provided a convenient spectral method for following the two conformational states of Trp191 since the binding of 1,2-dimethylimidazolium (DMI) to the Trp191 site in the open conformation results in an easily detectable spectral shift to a low-spin signal. In these studies, it was necessary to mutate Phe202 to Gly to sufficiently destabilize the Trp191 loop such that the "open" conformation could be crystallized and its structure determined (*36*). Since the mutations required to form the cation site in CCPK2 involve the same loop responsible for the open/close equilibrium described by Cao et al. (*36*) (residues 190−195), we reasoned that the 190−195 segment might be less stable in CCPK2 than in WTCCP. If so, then DMI should bind in the Trp191 pocket more readily in the CCPK2 mutant than in WTCCP. As shown in Figure 6, this is precisely what is found. The CCPK2 mutant could be readily titrated with DMI very similar to what was observed by Cao

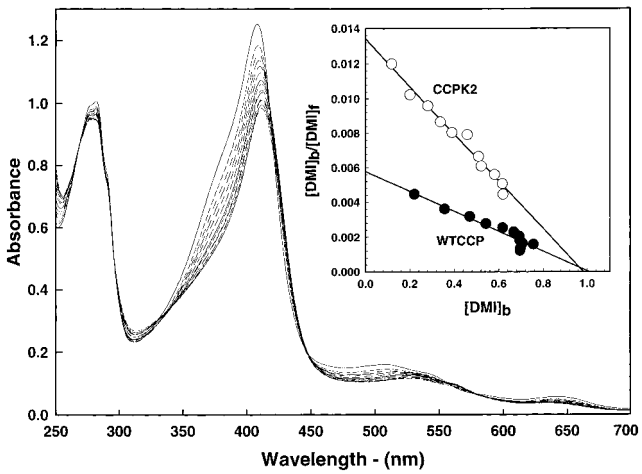

FIGURE 6: Binding of DMI to CCPK2 and WTCCP. A typical spectral titration curve for CCPK2 is shown. For CCPK2, about 30 min between addition of of DMI was required to achieve equilibrium while for WTCCP hours were required. Scatchard plots (inset) were used to determine the dissociation constant (K_d) by utilizing the difference absorbance (ΔAbs) at 408 nm. The fraction of DMI bound, $[DMI]_b$, was determined by extrapolating $1/\Delta A_{408}$ vs $1/[DMI]_t$ to infinite [DMI] assuming one binding site (*13*).

et al. (*36*), while WTCCP was quite stable to the addition of DMI. The estimated K_d based on double-reciprocal plots is 73.1 mM for CCPK2 and 172.4 mM for WTCCP. Consistent with the results of Cao et al. (*36*), the rate of DMI binding is extremely slow. For WTCCP, hours were required to achieve equilibrium between additions of DMI while only 30 min was required for CCPK2. These results are consistent with the following scheme proposed by Cao et al. (*36*):

$$\text{closed} \rightleftarrows \text{open} \overset{\text{DMI}}{\rightleftharpoons} \text{open}-\text{DMI}$$

It is clear that the mutations alone in CCPK2 result in a destabilization of the Trp191 pocket such that Trp191 can more readily adopt the "open" conformation near the surface. This is very likely the source of activity loss and decrease in the EPR signal of CCPK2 without added K^+. Further addition of K^+ to the "closed" conformation in CCPK2 is the source of the additional loss in activity due to electrostatic destabilization of the Trp191 cationic radical.

DISCUSSION

The excellent correlation between $[K^+]$, the compound I EPR signal, and enzyme activity further supports our earlier view that the cation site modulates the reactivity of the Trp191 cation radical. The source of this modulation is electrostatic destabilization of the positive charge on the Trp191 cation radical owing to the presence of the K^+ cation ∼8 Å from the Trp. In our earlier work, we utilized electrostatic calculations to obtain a qualitative picture which indicated that the local electrostatic potential around Trp191 in CCPK2 is more positive than in WTCCP. That the electrostatic potential controls the reactivity of Trp191 now has received further support by more sophisticated calculations comparing CCP with APX (*15*).

The steady-state kinetic analysis and stopped-flow studies indicate that it is reduction in the electron-transfer rate that is responsible for the loss in activity and further support the essential role that Trp191 plays in both the first and second

electron-transfer steps. There is a longstanding debate on whether CCP has one or two electron-transfer sites, one which leads to reduction of the Trp191 radical and the second which leads to reduction of the Fe^{4+}═O center. There is little doubt that CCP has at least two sites for binding cyt *c* (*37*, *38*), but this does not necessarily mean there are two sites of electron transfer. Studies where covalent tethering of cyt *c* to CCP using engineered sites designed to produce a covalent complex that mimics the noncovalent complex observed in the crystal structure (*8*) are relevant to the one- or two-site models. The covalent complex can undergo rapid intramolecular electron transfer but is inactive toward exogenous ferrocyt *c* at physiological ionic strength (*39*) which shows that the site required for interaction with cyt *c* has been blocked in the covalent complex. This supports the view that there is one physiologically important site of electron transfer as well as the following overall CCP electron-transfer process (*21*):

$$\mathrm{CCP}(\mathrm{Fe}^{4+}{=}\mathrm{O}\ \mathrm{Trp}^{\bullet+}) + \mathrm{e}^- \rightarrow \mathrm{CCP}(\mathrm{Fe}^{4+}{=}\mathrm{O}\ \mathrm{Trp}) \rightarrow \mathrm{CCP}(\mathrm{Fe}^{3+}\ \mathrm{Trp}^{\bullet+})$$

$$\mathrm{CCP}(\mathrm{Fe}^{3+}\ \mathrm{Trp}^{\bullet+}) + \mathrm{e}^- \rightarrow \mathrm{CCP}(\mathrm{Fe}^{3+}\ \mathrm{Trp})$$

In this scheme, the first electron reduces the Trp191 radical which is followed by an intramolecular electron transfer from Trp191 to Fe^{4+}═O, giving, once again, the Trp191 radical. The second electron then is utilized to reduce the Trp191 radical, thus completing the cycle which requires only one productive site of interaction between CCP and ferrocyt *c*.

A puzzling aspect of our present studies is why the mutations themselves without K^+ result in a large drop in activity. Since CCPK2 adheres less tightly to a cyt *c* affinity column, part of the loss in activity could be due to interference with proper formation of the CCP−cyt *c* complex. One fault in this argument is the proteins are in different redox states on the affinity column than they are in the conditions of steady-state analysis. Moreover, the very similar Eadie−Hofstee plots for WTCCP and CCPK2 and the fact that the break between the two slopes occurs at nearly the same concentration, ∼9 μM of ferrocyt *c* (Figure 4a,b), indicate that CCPK2 most likely forms a similar complex as WTCCP at low ionic strength used in the steady-state experiments. Interference with cyt *c* binding, however, does not explain the loss in the Trp191 radical signal due to the mutations alone. The spectral titration work with DMI provides a very plausible explanation. It is known that DMI can bind in the Trp191 pocket when CCP is in the open conformation where Trp191 is exposed to the molecular surface owing to a large movement of residues 190−195 (*36*). Since CCPK2 can bind DMI more readily than WTCCP, it must be that the 190−195 loop in CCPK2 is less stable. Therefore, there are three sources of activity loss. One is destabilization of residues 190−195 such that Trp191 adopts the "out" conformation more readily. The second is the binding of cations to CCP to the "in" conformation which destabilizes the Trp191 cation radical via long-range electrostatic effects. The third is a possible alteration and weakening of the CCP−cyt *c* complex. The obvious next step is to find ways to stabilize residues 190−195 in the CCPK2 mutant such that full or nearly full activity is restored in the absence of K^+. This would result in a peroxidase that exhibits very large differences in activity ± cations, giving a sensitive cation sensor and a cation-controlled molecular switch.

ACKNOWLEDGMENT

We thank C. S. Raman for his valuable assistance in performing the EPR experiment and for his useful advice and critique. C.A.B. thanks Dr. David Mandelman for his continuing work on APX and the insight he has provided and Joumana Jamal for her verification of some of the data presented here.

REFERENCES

1. Dolphin, D., Forman, A., Borg, D. C., Fajer, J., and Felton, R. H. (1971) *Proc. Natl. Acad. Sci. U.S.A. 68*, 614−618.
2. Yonetani, T. (1976) in *The Enzymes* (Boyer, B., Ed.) pp 345−361, Academic Press, Orlando, FL.
3. Sivaraja, M., Goodin, D. B., Smith, M., and Hoffman, B. M. (1989) *Science 245*, 738−740.
4. Huyett, J. E., Doan, P. E., Gurbriel, R., Houseman, A. L. P., Sivaraja, M., Goodin, D. B., and Hoffman, B. M. (1995) *J. Am. Chem. Soc. 117*, 9033−9041.
5. Goodin, D., and McRee, D. E. (1993) *Biochemistry 32*, 3313−3324.
6. DePillis, G. D., Sishta, B. P., Mauk, A. G., and Ortiz de Montellano, P. R. (1991) *J. Biol. Chem. 266*, 19334−19341.
7. Stemp, E. D., and Hoffman, B. M. (1993) *Biochemistry 32*, 10848−10865.
8. Pelletier, H., and Kraut, J. (1992) *Science 258*, 1748−1755.
9. Patterson, W. R., and Poulos, T. L. (1995) *Biochemistry 34*, 4331−4341.
10. Pappa, H., Patterson, W. H., and Poulos, T. L. (1996) *J. Biol. Inorg. Chem. 1*, 66−66.
11. Mauro, J. M., Fishel, L. A., Hazzard, J. T., Meyer, T. E., Tollin, G., Cusanovich, M. A., and Kraut, J. (1988) *Biochemistry 27*, 6243−6256.
12. Miller, M. A., Han, G. W., and Kraut, J. (1994) *Proc. Natl. Acad. Sci. U.S.A. 91*, 11118−11122.
13. Fitzgerald, M. M., Churchill, M. J., McRee, D. E., and Goodin, D. B. (1994) *Biochemistry 33*, 3807−3818.
14. Bonagura, C. A., Sundaramoorthy, M., Pappa, H. S., Patterson, W. R., and Poulos, T. L. (1996) *Biochemistry 35*, 6107−6115.
15. Jensen, G. M., Bunte, S. W., Warshel, A., and Goodin, D. B. (1998) *J. Phys. Chem. B 102*, 8221−8228.
16. Patterson, W. R., Poulos, T. L., and Goodin, D. B. (1995) *Biochemistry 34*, 4342−4345.
17. Fishel, L. A., Villafranca, J. E., Mauro, J. M., and Kraut, J. (1987) *Biochemistry 26*, 351−360.
18. Choudhury, K., Sundaramoorthy, M., Hickman, A., Yonetani, T., Woehl, E., Dunn, M. F., and Poulos, T. L. (1994) *J. Biol. Chem. 269*, 20239−20249.
19. Yonetani, T. (1966) *Biochem. Prep. 11*, 14−20.
20. Fowler, R. M., and Bright, H. A. (1935) *J. Res. Natl. Bur. Stand. 15*, 493−575.
21. Hahm, S., Miller, M. A., Geren, L., Kraut, J., Durham, B., and Millett, F. (1994) *Biochemistry 33*, 1463−1480.
22. Hahm, S., Green, L., Durham, B., and Millett, F. (1993) *J. Am. Chem. Soc. 115*, 3372−3373.
23. Edwards, S. L., and Poulos, T. L. (1990) *J. Biol. Chem. 265*, 2588−2595.
24. Sundaramoorthy, M., Choudhury, K., Edwards, S. L., and Poulos, T. L. (1991) *J. Am. Chem. Soc. 113*, 7755−7757.
25. Otwinoski, Z., and Minor, W. (1996) *Methods Enzymol. 276*, 307−326.
26. Brunger, A. T. (1992) Yale University Press, New Haven, CT.
27. Brunger, A. T. (1992) *Nature 355*, 472−475.
28. Jones, T. A. (1985) *Methods Enzymol. 115*, 157−171.

29. Mandelman, D., Sshwarz, F. P., Li, H., and Poulos, T. L. (1998) *Protein Sci. 7*, 2089−2098.
30. Finzel, B. C., Poulos, T. L., and Kraut, J. (1984) *J. Biol. Chem. 259*, 13027−13036.
31. Edwards, S. L., Nguyen, H. X., Hamlin, R. C., and Kraut, J. (1987) *Biochemistry 26*, 1503−1511.
32. Fulop, V., Phizackerley, R. P., Soltis, S. M., Clifton, I. J., Wakatsuki, S., Erman, J., Hajdu, J., and Edwards, S. L. (1994) *Structure 2*, 201−208.
33. Edwards, S. L., Poulos, T. L., and Kraut, J. (1984) *J. Biol. Chem. 259*, 12984−12988.
34. Kang, C. H., Ferguson-Miller, S., and Margoliash, E. (1977) *J. Biol. Chem. 252*, 919−926.
35. Corin, A. F., McLendon, G., Zhang, Q., Hake, R. A., Falvo, J., Lu, K. S., Ciccarelli, R. B., and Holzschu, D. (1991) *Biochemistry 30*, 11585−11595.
36. Cao, Y., Musah, R. A., Wilcox, S. K., Goodin, D. B., and McRee, D. E. (1998) *Protein Sci. 7*, 72−78.
37. Zhou, J. S., and Hoffman, B. M. (1994) *Science 265*, 1693−1696.
38. Mauk, M. R., Ferrer, J. C., and Mauk, A. G. (1994) *Biochemistry 33*, 12609−12614.
39. Pappa, H. S., Tajbaksh, S., Saunders, A. J., Pielak, G. J., and Poulos, T. L. (1996) *Biochemistry 35*, 4837−4845.

BI982996K